

# Long Baseline Neutrino Physics: From Fermilab to Kamioka

Fritz DeJongh\*  
*Fermilab*

October 29, 2018

## Abstract

We have investigated the physics potential of very long baseline experiments designed to measure  $\nu_\mu \rightarrow \nu_e$  oscillation probabilities. The principles of our design are to tune the beam spectrum to the resonance energy for the matter effect, and to have the spectrum cut off rapidly above this energy. The matter effect amplifies the signal, and the cut-off suppresses backgrounds which feed-down from higher energy. The signal-to-noise ratio is potentially better than for any other conventional  $\nu_\mu$  beam experiment.

We find that a beam from Fermilab aimed at the Super-K detector has excellent sensitivity to  $\sin^2(2\theta_{13})$  and the sign of  $\Delta M^2$ . If the mass hierarchy is inverted, the beam can be run in antineutrino mode with a similar signal-to-noise ratio, and event rate 55% as high as for the neutrino mode.

Combining the Fermilab beam with the JHF-Kamioka proposal adds very complementary information. We find good sensitivity to maximal CP violation for values of  $\sin^2(2\theta_{13})$  ranging from 0.001 to 0.05.

---

\*fritzd@fnal.gov

# 1 Introduction

Measurements of the atmospheric neutrino flux with the Super-Kamiokande detector have shown that the deficit of muon neutrinos depends on the zenith angle as expected for neutrino oscillations [1]. This result combined with many other experimental constraints provides strong evidence for  $\nu_\mu \rightarrow \nu_\tau$  oscillations, with mixing  $> 0.88\%$  (90% C.L.) and  $\Delta M^2$  in the range  $(1 - 5) \times 10^{-3} \text{ eV}^2$  [2].

Efforts to study these oscillations with accelerator-produced neutrinos are in progress, using  $\nu_\mu$  beams produced from pion decay. The K2K collaboration has detected neutrino interactions in the Super-K detector using a neutrino beam from KEK 250 km distant. They report a deficit of events compared to the expectation with no oscillations [3]. The MINOS experiment is under construction, and will use an Iron/scintillator detector 730 km distant from a neutrino beam produced at Fermilab [4]. These experiments are expected to confirm that the  $\nu_\mu$  disappearance has the  $L/E$  dependence expected for oscillations, and improve the precision on  $\Delta M^2$ .

Measurements of solar neutrino fluxes also provide evidence for neutrino oscillations, usually explained as  $\nu_e \rightarrow \nu_\mu$  oscillations with  $\Delta m^2$  much smaller than the  $\Delta M^2$  for atmospheric oscillations. The Large Mixing Angle (LMA) solution is strongly favored by the data, with  $\Delta m^2$  in the range  $(3 - 25) \times 10^{-5} \text{ eV}^2$  [5]. The KamLAND [6] and Borexino [7] experiments, currently under construction, are expected to test the LMA solution and better constrain the mixing parameters.

The atmospheric and solar neutrino oscillations can be simultaneously explained with mixing in a three-flavor model: The the three known flavors of neutrinos,  $\nu_e$ ,  $\nu_\mu$ , and  $\nu_\tau$ , are mixtures of mass eigenstates  $\nu_1$ ,  $\nu_2$ , and  $\nu_3$ . The data require a mass hierarchy, with  $|m_3 - m_2| \gg |m_2 - m_1|$ . The hierarchy can be “normal”, with  $m_3 > m_2$ , or “inverted”, with  $m_2 > m_3$ . We identify  $\Delta M^2 = m_3^2 - m_2^2$  and  $\Delta m^2 = m_2^2 - m_1^2$ .

While  $\nu_\mu \rightarrow \nu_e$  oscillations are mainly associated with solar oscillations, they can also occur at the atmospheric frequency if there is a  $\nu_3$  component in the  $\nu_e$  eigenstate. Reactor experiments have placed limits on the size of this mixing, resulting in the limit  $\sin^2(2\theta_{13}) < 0.1$  [8, 9]. If  $\sin^2(2\theta_{13}) > 0$  can be detected, the phenomenology of  $\nu_\mu \rightarrow \nu_e$  oscillations becomes very rich:

- Interference between the solar and atmospheric oscillation amplitudes can result in large CP violation [10].

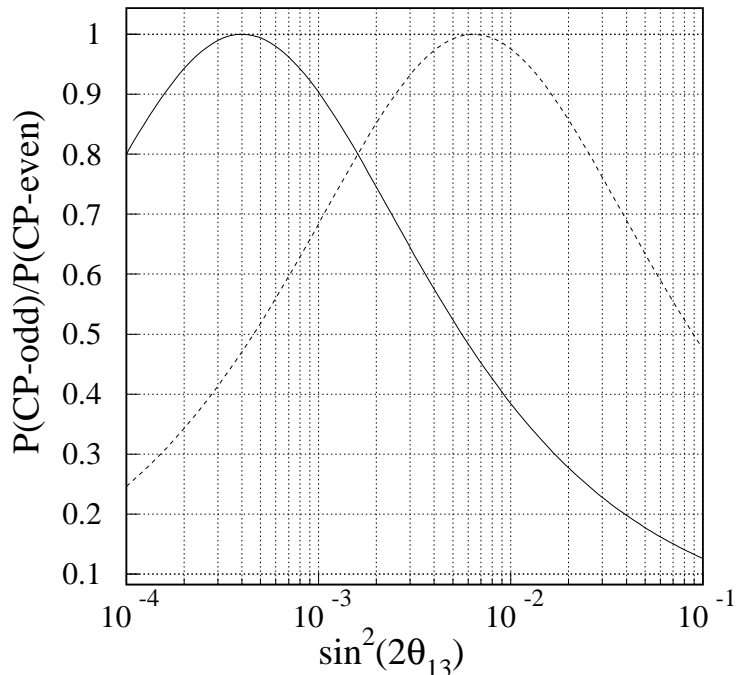


Figure 1: CP asymmetry at the peak of the atmospheric oscillation for the parameters of Table 1. Solid line is for  $\Delta m^2 = 5.0 \times 10^{-5} \text{ eV}^2$ , and dashed line is for  $\Delta m^2 = 2.0 \times 10^{-4} \text{ eV}^2$ .

- Matter effects can modify the oscillation probability, depending on the sign of  $\Delta M^2$  [11, 12, 13].

To study these effects on the oscillation probability, we use the parametrization of Ref. [14], with the oscillation parameters of Table 1 as defaults. For example, Fig. 1 shows the possible CP asymmetry as a function of  $\sin^2(2\theta_{13})$ , at the peak of the atmospheric oscillations. While the mixing in solar oscillations is greater than in atmospheric oscillations, the solar oscillations develop much more slowly, so the two amplitudes for  $\nu_\mu \rightarrow \nu_e$  can be comparable at atmospheric baselines. We note that maximal CP asymmetry is a possibility: There could be a large signal for neutrinos and no signal at all for antineutrinos, or vice-versa.

Given the potential for profound insights into fundamental physics, most studies of future neutrino oscillation experiments with conventional  $\nu_\mu$  beams have focused on  $\nu_\mu \rightarrow \nu_e$  oscillations. A wide variety of neutrino energies and detector technologies have been considered in Refs. [15, 16, 17, 18].

$\sin^2(2\theta_{13})$	variable
$\Delta M^2$	$3.5 \times 10^{-3} \text{ eV}^2$
$\Delta m^2$	$5.0 \times 10^{-5} \text{ eV}^2$
$\sin^2(2\theta_{23})$	1.0
$\sin^2(2\theta_{12})$	0.8
$\delta$	$\pi/2$

Table 1: Default oscillation parameters

The potential of low energy neutrino beams combined with large water-erenkov detectors has been explored for beams based at JHF [19], CERN [20], and Fermilab [18] and baselines of 100 to 300 km. These low energy approaches have the advantage of very low backgrounds, and have excellent sensitivity to very small  $\nu_e$  appearance signals. They have the disadvantage that matter effects are too small to disentangle from CP violating effects, but are still large enough that ambiguities from the unknown sign of  $\Delta M^2$  affect the ability of the experiment to establish CP violation [21].

The potential of higher energy neutrino beams with very long baseline ( $L > 7000$  km) has been explored in Refs. [15, 18]. The backgrounds in water cerenkov detectors are larger for higher neutrino energies. However, the  $\nu_\mu \rightarrow \nu_e$  signal at these baselines can be highly amplified by matter effects, improving the signal-to-background ratio [11, 12, 13]. Also, the amplified signal depends mostly on atmospheric oscillations, with solar oscillations playing a much smaller role than with shorter baselines.

From this summary of short- and long-baseline neutrino oscillation experiments, we see that they can play very complimentary roles. The short-baseline experiment measures a CP-violating combination of atmospheric and solar oscillations. The long-baseline experiment determines the sign of  $\Delta M^2$ , constrains the matter effects, and constrains the size of the atmospheric  $\nu_\mu \rightarrow \nu_e$  oscillation alone.

We propose herein an optimized long-baseline experiment to complement a short-baseline experiment. For concreteness, we assume a target detector at the Kamioka site in Japan, where the Super-K detector already exists. The JHF-Kamioka proposal [19] uses the Super-K detector for the first phase, and for the second phase assumes construction of a new detector with 40 times more fiducial mass. We assume that this detector will be used as the target for two neutrino beams: One from JHF, with a baseline of 295 km, and one from Fermilab, with a baseline of 9300 km. The concept of our proposal

does not depend on the details of this choice, and could be adapted for other locations. The main principles of our proposal are:

1. Combine information from very short and very long baselines in order to determine the mass hierarchy and CP-violating oscillation parameters.
2. Match the spectrum of the long-baseline neutrino beam to the energy at which matter effects produce the maximum amplification of the signal.
3. Design the long-baseline neutrino beam to have an energy spectrum with a rapid cut-off above the signal region. Since most backgrounds feed-down from the neutrino energy to a lower visible energy, this reduces the background in the signal region.

## 2 The $\nu_\mu \rightarrow \nu_e$ probability at 9300 km

We start in the “leading approximation” which parametrizes oscillations driven by the atmospheric  $\Delta M^2$  and neglects oscillations driven by the solar  $\Delta m^2$ . The  $\nu_\mu \rightarrow \nu_e$  probability can then be written as

$$P(\nu_\mu \rightarrow \nu_e) = R_m^2 \sin^2 \theta_{23} \sin^2 2\theta_{13} \sin^2 \left( \frac{1.267 \Delta M^2 L}{R_m E_\nu} \right). \quad (1)$$

The effects of interaction with matter are included in the parameter  $R_m$ . In vacuum,  $R_m = 1$ . For positive  $\Delta M^2$ , there is a resonant energy at which there is full mixing, with  $R_m = 1/(\sin \theta_{23} \sin 2\theta_{13})$ . For antineutrinos, this resonance occurs for negative  $\Delta M^2$ . Since we’re considering the case  $\sin^2 2\theta_{13} < 0.1$ , the oscillation length becomes very long, and for terrestrial baselines we can expand the probability to first order in  $L$ :

$$P(\nu_\mu \rightarrow \nu_e) = \sin^2 \theta_{23} \sin^2 2\theta_{13} \left( 1.267 \Delta M^2 \frac{L}{E_\nu} \right)^2. \quad (2)$$

Since the flux is proportional to  $1/L^2$ , we find that the number of expected signal events is independent of distance. Since background rates decline with  $L^2$ , longer baselines will provide better signal to noise. For negative  $\Delta M^2$ , the signal would be suppressed and unobservable.

Fig. 2 shows  $P(\nu_\mu \rightarrow \nu_e)$  as a function of neutrino energy for a baseline of 9300 km,  $\Delta M^2 = 3.5 \times 10^{-3} \text{ eV}^2$ , and  $\sin^2 2\theta_{13} = 0.01$ . We see that the

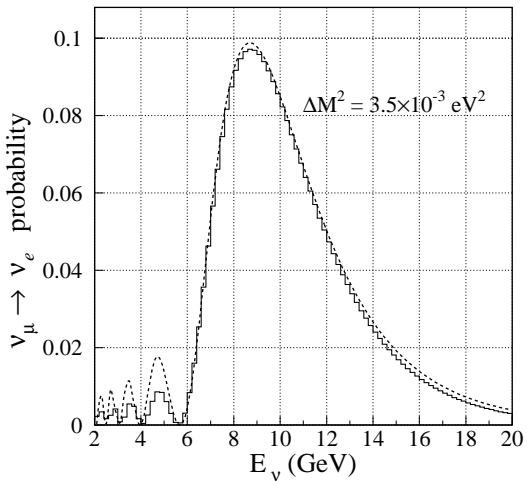


Figure 2: Oscillation probability as a function of energy, for  $L = 9300$  km,  $\sin^2(2\theta_{13}) = 0.01$ , and neglecting solar oscillations. Solid histogram is from a numerical calculation [22], dashed line is from the analytical approximation of Ref. [14], with the matter parameter  $A$  set to  $1.75 \times 10^{-4}$  eV<sup>2</sup>/GeV.

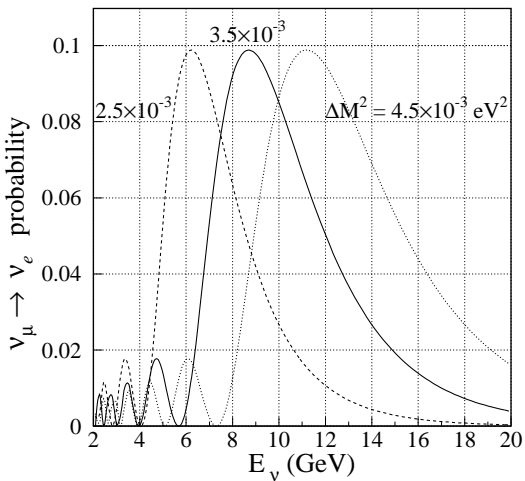


Figure 3: Oscillation probability as a function of energy, for three different values of the atmospheric  $\Delta M^2$  and parameters of Fig. 2.

resonant energy is in the range 8 to 10 GeV. At this energy, the oscillation probability is 20 times the maximum probability occurring in vacuum.

Fig. 2 also compares a numerical calculation [22] of the exact theory incorporating the density variation of the Earth, with an analytical approximation [14] using an average density. The agreement is excellent in the energy range of interest, and we use the analytical approximation for the rest of this paper. Refs. [11, 12] have also shown that using an average density is a good approximation for similar parameters.

Fig. 3 shows  $P(\nu_\mu \rightarrow \nu_e)$  for different values of  $\Delta M^2$ . The resonant energy is proportional to  $\Delta M^2$ , while the maximum oscillation probability is constant.

The analytical approximation of Ref. [14] can also be used to include non-leading terms. The amplification occurs mainly for the leading terms, so

the oscillation probability for a 9300 km baseline is dominated by the leading terms much more than for shorter baselines.

### 3 The neutrino beam

Our starting point for the neutrino beamline design is the NuMI beamline at Fermilab, which is currently under construction. In the NuMI beamline, 120 GeV protons from the Main Injector collide with a target which is designed for an average power of 0.4 MW. Pions produced in the target are focused and charge-selected in a double horn system, and then decay in a 675 m decay tunnel. This produces a beam consisting of mainly  $\nu_\mu$ . Different configurations of the target and horns produce spectra peaking at different energies. There is a small  $\nu_e$  contamination arising from the decay of kaons produced in the target, and the decay of muons produced in pion decays. The level of this contamination varies from 0.6 to 1%, depending on the configuration.

The accelerator used to inject protons into the Main Injector is the Booster ring, which accelerates protons up to 8 GeV. Proton drivers with power of 1 MW or more are currently being designed [23, 24]. With a proton driver replacing the Booster, the Main Injector would be capable of delivering 2 MW of proton power to target. In the case of the linac option for the proton driver, it may be possible to deliver this power at any proton energy less than 120 GeV [24].

To aim a neutrino beam from Fermilab to the Kamioka site, the decay tunnel must be angled downwards  $46^\circ$  from the horizontal. At the Fermilab site, the decay tunnel must fit within a 200 m vertical depth in order to be within rock favorable for construction and to avoid a water aquifer. This limits the length of the decay tunnel, and reduces the efficiency for pions to decay and produce neutrinos. The length is further reduced by the vertical space needed to bend the protons down to the target, and the space needed for the target and focusing, and beam dump at the end of the tunnel.

As discussed in Sect. 5, most backgrounds for our measurement feed-down from the neutrino energy to a lower visible energy, while for the signal the entire neutrino energy is visible. Backgrounds in the signal region tend to arise from neutrinos with higher energy. Therefore, our goal for the neutrino beamline is to produce a spectrum which peaks at the energy for the maximum oscillation probability in Fig. 3, and falls off quickly at higher energy.

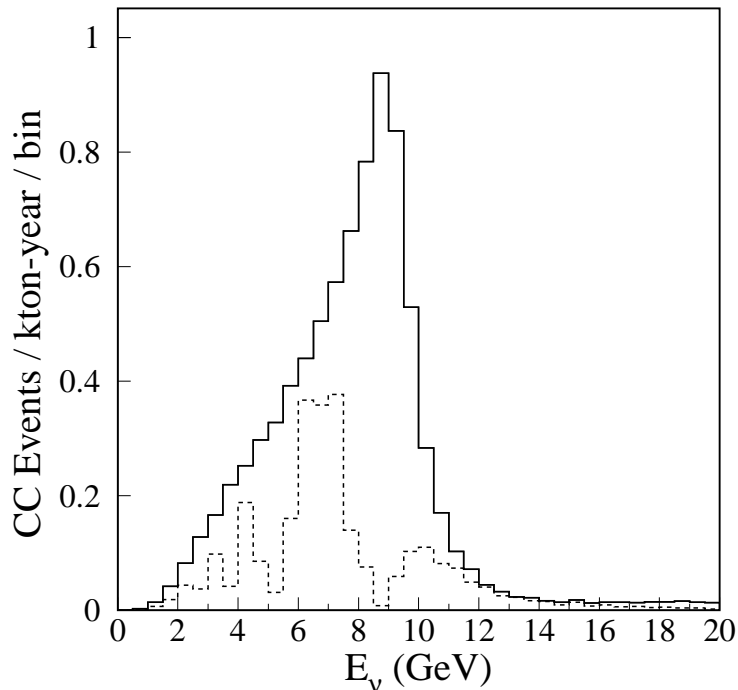


Figure 4: Solid line: Spectrum of interacting  $\nu_\mu$  CC events at the Kamioka site, assuming no oscillations. Dashed line includes effects of  $\nu_\mu$  disappearance from oscillations. We note that the second disappearance peak happens to occur at the peak of the spectrum.

A saw-tooth shape would be ideal. The lack of a high-energy tail might also simplify the radiation shielding requirements relative to NuMI.

The beamline will need to be tuned for the actual value of  $\Delta M^2$  when it is better known; for now we assume  $\Delta M^2 = 3.5 \times 10^{-3} \text{ eV}^2$ , and aim for a peak energy of 9 GeV.

We have used the NuMI fast beamline simulation to produce a candidate beamline design. For the following, we apply a scaling factor of 1.25 needed to bring the fast simulation into agreement with the full simulation of the medium- and high-energy NuMI configurations [25]. Starting with a standard NuMI configuration, we have made the following changes:

1. Use 60 GeV protons on target instead of 120 GeV. This reduces the cost of the bending magnets, and allows the bend to occur in less vertical space. We assume a field of 6 T for the bending magnets.



2. We assume the accelerator complex is upgraded to provide 2 MW of proton power from the Main Injector.
3. Change the target and horn configuration to produce a spectrum peaking at 10 GeV.
4. Add a small dipole bend after the horns, to bend 20 GeV pions by  $0.5^\circ$ . This allows the higher energy pions to be filtered out, and reduces some of the  $\nu_e$  component by filtering out neutral kaons.

The resulting spectrum is shown in Fig. 4, and has the basic properties we were aiming for. The  $\nu_\mu$  spectrum including oscillation effects is also shown. In an interesting coincidence, the 2nd disappearance peak happens to occur at the peak of the spectrum. The length of the pion decay tunnel is 210 m, and the decay efficiency is 37% what it would be for a NuMI length tunnel.

The event rates do not depend critically on the specifics of the design. For example, if we need to use 120 GeV protons to get the full beam power, the pion decay efficiency relative to NuMI decreases only to 35%. Or, if we use 2 T bending magnets and 60 GeV protons, the relative efficiency decreases to 33%.

Ref. [26] has also presented beamline simulations producing energy spectra with sawtooth shapes, using quadrupole magnets instead of horns to focus the pions.

### 3.1 Flux normalization

Since the use of space for a near detector would further reduce the efficiency of the beamline, we have assumed that there will be no near detector and the flux can be normalized using data in the far detector. As shown in Fig. 4, we expect a large rate of  $\nu_\mu$  charged-current interactions in the far detector, and this can in principle be used to normalize the flux. The systematic limitations of this procedure will have to be studied with a detailed simulation. It's possible that neutral-current interactions or  $\nu_\tau$  charged-current interactions might also be used to help measure the flux.

### 3.2 Running with antineutrino beams

The neutrino beamline can be converted into an antineutrino beamline by reversing the polarity of the focusing horns and bending magnet. Since the

antineutrino cross-section is smaller than the neutrino cross-section, and  $\pi^-$  production in the proton target is suppressed relative to  $\pi^+$  production, event rates in the far detector are typically 1/3 of those in neutrino beams. The intrinsic  $\nu_e$  and  $\bar{\nu}_e$  backgrounds tend to be worse as well. These problems are mitigated by the following effects:

- As discussed in Sect. 4, the efficiency of reconstructing  $\bar{\nu}_e$  events is higher than for  $\nu_e$  events. After reconstruction and event selection cuts, the antineutrino rate will be about 55% of the neutrino rate.
- The dipole bend helps remove neutral kaons and  $K^+$  in the pion decay tunnel, removing the  $\nu_e$  component of the beam. The remaining  $\bar{\nu}_e$  component will be comparable to the  $\nu_e$  component of the neutrino beam.

## 4 The $\nu_e$ signal

The  $\nu_e$  signal is detected from charged-current (CC) interactions producing an electron along with a hadronic shower with energy  $E_{\text{had}}$ . The visible energy of the event,  $E_{\text{vis}}$ , (the energy not carried away by neutrinos) is equal to the neutrino energy. The differential cross-section in terms of the variable  $y = E_{\text{had}}/E_\nu$ , normalized to 1, can be approximately parametrized by [29]:

$$\frac{d\sigma_\nu}{dy} = \frac{15}{16} \left( 1 + \frac{(1-y)^2}{5} \right). \quad (3)$$

For antineutrinos, the parametrization is:

$$\frac{d\sigma_{\bar{\nu}}}{dy} = \frac{15}{8} \left( \frac{1}{5} + (1-y)^2 \right). \quad (4)$$

We will model the efficiency of detecting a  $\nu_e$  CC event by assuming the fiducial mass of the detector for the target mass, and by requiring the production of an electron above some threshold  $E$ . The probability of a  $\nu_e$  with energy  $E_\nu$  generating an electron above a threshold  $E$  is:

$$p_{cc} = \frac{15}{16} \left( \frac{16}{15} - \frac{E}{E_\nu} - \frac{1}{15} \left( \frac{E}{E_\nu} \right)^3 \right). \quad (5)$$

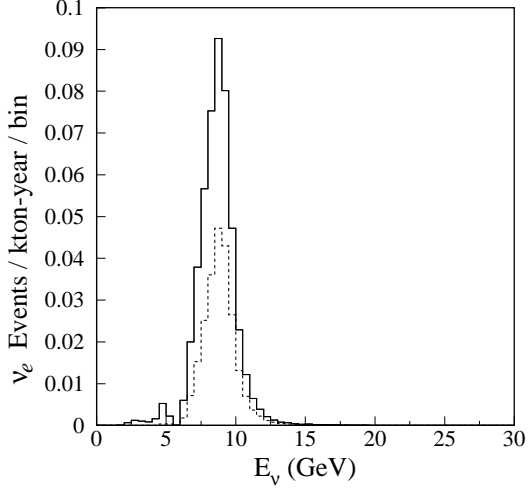


Figure 5: Solid line: Spectrum of interacting  $\nu_e$  CC events at the Kamioka site, assuming the oscillation parameters of Fig. 2. Dashed line includes effects of cuts described in Sect. 4.

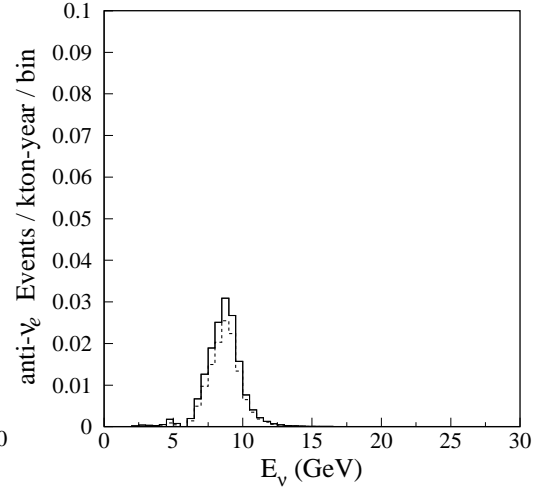


Figure 6: Solid line: Spectrum of interacting  $\bar{\nu}_e$  CC events at the Kamioka site, assuming the oscillation parameters of Fig. 2. Dashed line includes effects of cuts described in Sect. 4. The rate after cuts is 55% of the rate for  $\nu_e$  CC events.

For antineutrinos, the parametrization is:

$$p_{cc} = \frac{15}{8} \left( \frac{8}{15} - \frac{1}{5} \frac{E}{E_\nu} - \frac{1}{3} \left( \frac{E}{E_\nu} \right)^3 \right). \quad (6)$$

For neutrinos, we choose the following cuts for the threshold  $E$ :

1.  $E > 4.5$  GeV.
2.  $E/E_{\text{vis}} > 0.45$ .

Fig. 5 shows the  $\nu_e$  CC energy spectrum at the Kamioka site, assuming the neutrino beam described in Sect. 3, and the neutrino oscillation parameters of Fig. 2. The dashed line of Fig. 5 shows the effect of the above cuts. The average efficiency of these cuts is 50%. With these cuts, we find 0.21 events

in the signal region, per kton-year of exposure, where the signal region is defined as energy between 7 and 10.5 GeV.

The  $y$ -distribution for antineutrinos is more peaked towards zero than for neutrinos, as described by Eqs. (3) and (4). Therefore, for the same NC background fraction,  $\bar{\nu}_e$  CC events can be selected with more efficient cuts. For neutrinos, we choose the following cuts for the threshold  $E$ :

1.  $E > 3.3$  GeV.
2.  $E/E_{\text{vis}} > 0.33$ .

Fig. 6 shows the  $\bar{\nu}_e$  CC energy spectrum at the Kamioka site, assuming the neutrino beam described in Sect. 3, and the neutrino oscillation parameters of Fig. 2 with negative  $\Delta M^2$ . The dashed line of Fig. 6 shows the effect of the above cuts. The average efficiency of these cuts is 80%, producing an antineutrino signal rate 55% of the neutrino rate.

## 5 Backgrounds

### 5.1 Backgrounds from neutral-current events

Neutral pions are produced in the hadronic showers present in all neutrino interactions with nuclei. At high energies, the photons from the  $\pi^0 \rightarrow \gamma\gamma$  decay produce a single electromagnetic shower, which in water cerenkov detectors is indistinguishable from that of an electron. Neutral-current (NC) events with an energetic  $\pi^0$  constitute a major background to the  $\nu_e$  appearance signal. The visible energy of these events is given by  $yE_\nu$ , so they feed-down from the neutrino energy to a lower visible energy.

We have studied the production of neutral pions with the LEPTO program [27] which generates deep inelastic neutrino interactions and models the fragmentation of the hadronic component. There are several efforts underway to model resonance and quasi-elastic production, which we have not included, and which might account for roughly 15% of the cross-section in the energy range we are interested in [28]. However, we do expect the backgrounds to come more from high- $y$  events, or from feed-down from higher-energy neutrinos, where the fragmentation assumption is more applicable.

We find that Eq. (3) and Eq. (4) agree well with LEPTO-generated data for charged-current and neutral-current events.

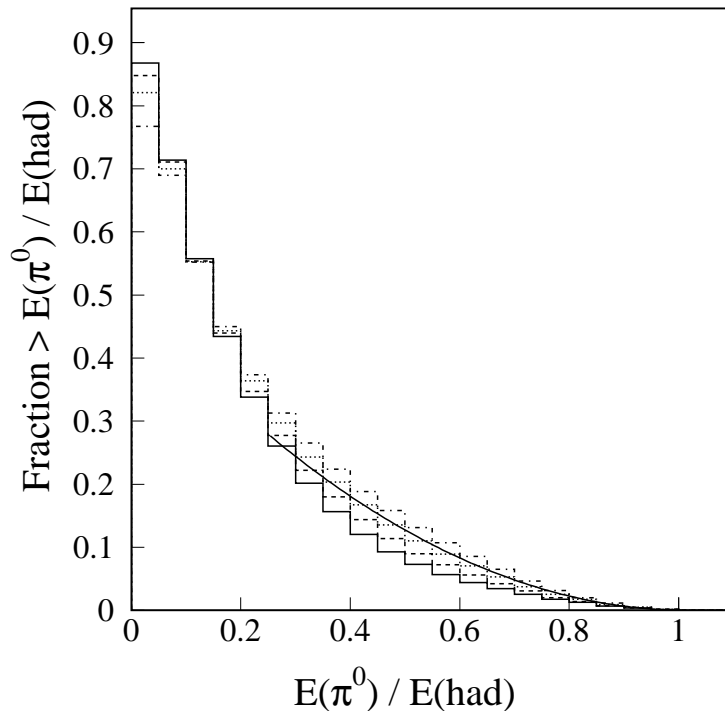


Figure 7: Integral plots of the  $E(\pi^0)/E(\text{had})$  distribution in neutrino interactions. The different histograms are for different ranges of hadronic energy: Solid: 20 to 25 GeV. Dashed: 15 to 20 GeV. Dotted: 10 to 15 GeV. Dot-Dashed: 5 to 10 GeV. The curve is our parametrization of this quantity.

The  $\pi^0$  fragmentation functions are roughly independent of hadronic energy. This is illustrated in Fig. 7, which shows integral plots of the  $E(\pi^0)/E(\text{had})$  distribution. The probability for a hadronic shower to produce a  $\pi^0$  with energy greater than a fraction  $x$  of  $E(\text{had})$  can be parametrized by:

$$p(x) = (0.49) - (0.96)x + (0.47)x^2. \quad (7)$$

For a given neutrino energy, we can use Eq. 3 to obtain the visible energy spectrum in NC interactions. For a given visible energy, we can then use Eq. 7 to calculate the probability that there will be a  $\pi^0$  above some cut-off energy. Thus, we can convolute an input neutrino spectrum into an output NC background spectrum.

Fig. 8 shows the NC background to the  $\nu_e$  signal, estimated with this

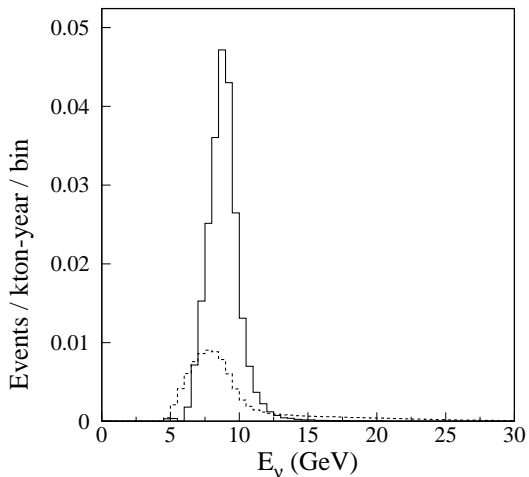


Figure 8: Solid line: Spectrum of  $\nu_e$  events with cuts from Fig. 5. Dashed line: Distribution of background from NC events.

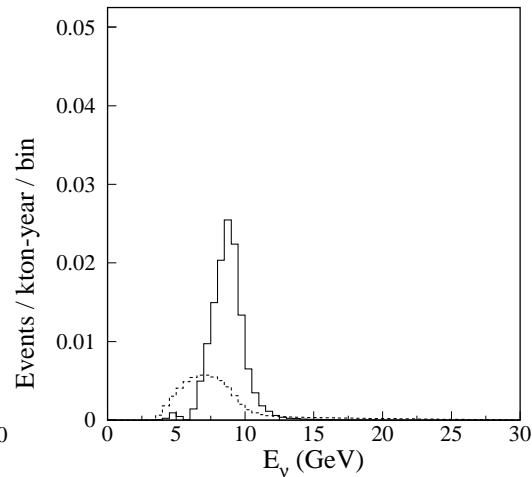


Figure 9: Solid line: Spectrum of  $\bar{\nu}_e$  events with cuts from Fig. 6. Dashed line: Distribution of background from NC events.

procedure with the cuts of Sect. 4. We find a background of 0.047 events per kton-year in the signal region, corresponding to  $f_B = 2.1\%$ , where  $f_B$  is the background fraction relative to the expected signal after cuts for a beam with 100%  $\nu_e$  [15]. Fig. 9 shows the same distributions for the  $\bar{\nu}_e$  signal. We obtain the same background fraction with a signal rate 55% of the  $\nu_e$  rate.

Since the direction of the incoming neutrino is known, and the outgoing neutrino can carry away transverse energy, the direction of the observed energy flow might also be used to further reduce NC background. A detailed simulation will be needed to investigate this possibility.

## 5.2 Background from $\nu_\mu$ charged-current interactions

In this analysis, we assume that all  $\nu_\mu$  CC events can be rejected due to the presence of a muon, and only consider the  $\pi^0$  background from NC events. For high- $y$  events however, the muon will have low energy and can easily be missed, while the hadronic shower has most of the energy of the neutrino. Neutral pions from these hadronic showers will generate backgrounds the same as for neutral currents. Fortunately, as illustrated in Fig. 4, the  $\nu_\mu$  flux is very low in the signal region. This is true for other values of  $\Delta M^2$  as well.

So, we expect this source of background to be negligible compared to the background from neutral current events.

### 5.3 Background from $\nu_\tau$ charged-current interactions

At the peak energy for the  $\nu_e$  signal, most of the  $\nu_\mu$  have oscillated into  $\nu_\tau$ , so  $\nu_\tau$  CC interactions are a potentially serious source of background. However, at this energy the  $\nu_\tau$  CC cross-section is only  $\approx 8\%$  of the  $\nu_e$  CC cross-section. The decay mode  $\tau \rightarrow e\nu\bar{\nu}$  produces a real electron background, but the branching ratio is only 18%. Neutral pions in  $\nu_\tau$  CC events can also produce backgrounds. Since all these events have an escaping neutrino from the  $\tau$  decay, these backgrounds feed-down to lower visible energy. As long as we keep the high energy tail of the neutrino beam suppressed, we expect this source of background to be small. However, the cuts needed to suppress this background need more study with a detailed simulation.

### 5.4 Intrinsic $\nu_e$ backgrounds

As discussed in Sect. 3 the neutrino beam has a small amount of  $\nu_e$  contamination. The dipole bend in the beamline can help reduce this background by eliminating neutral kaons in the beamline. Also, the  $\nu_e$  energy spectrum is very broad, while the signal region is narrow. The intrinsic  $\nu_e$  background as a function of the energy width of the beam has been studied in Ref. [15], showing that it is greatly reduced for narrow beams. Therefore, we expect this background also to be very small.

## 6 Comparison with the JHF-Kamioka project

The first stage of the JHF-Kamioka project uses a 0.75 MW proton driver to generate a neutrino beam aimed at the Super-Kamiokande detector. In phase 2, the proton power is increased to 4 MW, and a new water cerenkov detector, called Hyper-K, is built with 40 times more fiducial mass.

With very similar mixing parameters as those used in Sect. 4, the JHF-Kamioka proposal obtains 0.11 events per kton-year in phase 1, compared to 0.21 for our proposal. The event rate for the Fermilab beam is 200% of the rate for the phase 1 JHF beam, and 40% of the rate for the phase 2 JHF beam.

The JHF-Kamioka project achieves a very low background rate:  $f_B = 0.51\%$ , compared to  $f_B = 2.5\%$  for the Fermilab beam, where  $f_B$  is the background fraction relative to the expected signal after cuts for a beam with 100%  $\nu_e$  [15]. However, the signal from the Fermilab beam is amplified by a factor of 20, so the effective background for comparison with the JHF beam is only 0.13%.

The signal region for the Fermilab beam is fairly narrow, between 7 and 10.5 GeV. The signal region for the JHF beam is defined as energy between 0.4 and 1.2 GeV. The average oscillation probability over the JHF spectrum is only 56% of the peak probability. This further accentuates the background advantage of the Fermilab beam.

## 7 Combined analysis of data from Fermilab and JHF beams

In the previous section, we showed that the Fermilab and JHF beams would have comparable performance. The JHF phase 2 beam has an advantage in rate, while the Fermilab beam has an advantage in background. However, the real advantage comes in combining information from the two beams. The first step will be the detection of  $\nu_\mu \rightarrow \nu_e$  oscillations and determination of the sign of  $\Delta M^2$ . The second step will be constraints on sub-leading effects such as CP violation.

### 7.1 Detecting $\nu_\mu \rightarrow \nu_e$ oscillations and the sign of $\Delta M^2$

Fig. 10 shows our estimates of the reach in  $\sin^2(2\theta_{13})$  for JHF and Fermilab beams with the Super-K detector, assuming positive  $\Delta M^2$ , and atmospheric oscillations only. The JHF curves are in reasonable agreement with curves in the JHF-Kamioka proposal [19]. If a signal appears with the JHF beam, it should be confirmed by the Fermilab beam within one year of running, otherwise  $\Delta M^2$  must be negative. It should then be possible to find the signal with the Fermilab beam in antineutrino mode. The performance of the Fermilab beam is excellent: 5 years of running yields a  $3\sigma$  reach of 0.003 in  $\sin^2(2\theta_{13})$ .

Fig. 11 shows a similar plot for the Hyper-K detector. A 5 year run should produce a  $3\sigma$  reach of 0.001 or better, with a strong dependence on the background level and systematic uncertainty.



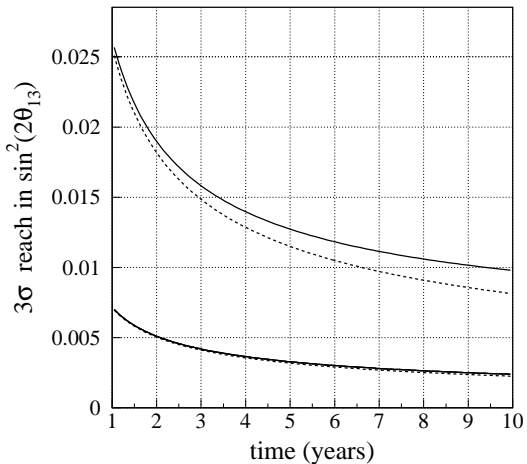


Figure 10: Reach in  $\sin^2(2\theta_{13})$  with Super-K detector. Upper curves are for JHF phase 1 beam, lower curves for Fermilab beam. Solid curves assume 10% systematic uncertainty on the background, dashed curves assume no systematic uncertainty. We assume positive  $\Delta M^2$ , and atmospheric oscillations only.

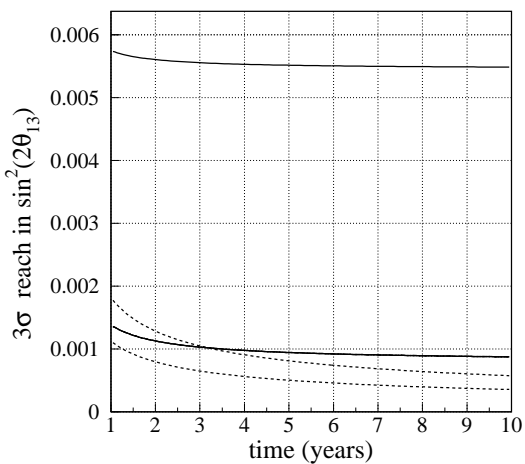


Figure 11: Reach in  $\sin^2(2\theta_{13})$  with Hyper-K detector. Upper curves are for JHF phase 2 beam, lower curves for Fermilab beam. Solid curves assume 10% systematic uncertainty on the background, dashed curves assume no systematic uncertainty. We assume positive  $\Delta M^2$ , and atmospheric oscillations only.

It is interesting that if  $\sin^2(2\theta_{13})$  is small enough for Eq. (2) to be valid, the long-baseline oscillation probability does not depend explicitly on the size of the matter effect for neutrinos at the resonant energy. If the peak energy for the matter resonance can be determined, the theory of matter effects can be tested and systematic uncertainties from matter effects can be kept small [13].

## 7.2 Constraints on the CP violating phase

The JHF-Kamioka phase 2 program assumes 2 years of neutrino running, and 6 years of antineutrino running. They have assumed the background will be very well constrained, and for our analysis we have assumed a 2% systematic uncertainty on the background. Except for the highest allowed values of

Beam	ye- ars	$\sin^2(2\theta_{13})$		
		0.01	0.05	0.001
Fermi	2	$0.104 \pm 0.0060$	$0.501 \pm 0.012$	$0.012 \pm 0.0034$
Fermi	8	$0.104 \pm 0.0032$	$0.501 \pm 0.0061$	$0.012 \pm 0.0021$
JHF $\nu$	2	$(7.9 \pm 0.37) \cdot 10^{-3}$	$(3.2 \pm 0.052) \cdot 10^{-2}$	$(1.5 \pm 0.32) \cdot 10^{-3}$
JHF $\nu$	8	$(7.9 \pm 0.25) \cdot 10^{-3}$	$(3.2 \pm 0.031) \cdot 10^{-2}$	$(1.5 \pm 0.24) \cdot 10^{-3}$
JHF $\bar{\nu}$	6	$(2.8 \pm 0.33) \cdot 10^{-3}$	$(1.8 \pm 0.044) \cdot 10^{-2}$	$(0.0 \pm 0.31) \cdot 10^{-3}$

Table 2: Expected oscillation probability measurements for the various beams and input values.

$\sin^2(2\theta_{13})$ , it will be necessary to either find a way to further reduce the background, or to determine the background to this level. For the Fermilab beam, we have assumed a 5% systematic uncertainty on the background, and an 8 year run.

We have neglected the systematic uncertainty on the flux prediction, but note that for the highest allowed values of  $\sin^2(2\theta_{13})$ , it will need to be constrained to 1%.

For the JHF beam, we have assumed the signal to background ratio in the antineutrino beam is the same as for the neutrino beam, and the 6 year exposure for the antineutrino beam is equivalent to 2 years with the neutrino beam. Without a dipole bend, it is likely that the backgrounds with the antineutrino beam will in fact be much worse. As an alternative, we have considered running for 8 years with the JHF neutrino beam.

We have assumed the parameter values in Table 1, and  $\sin^2(2\theta_{13}) = 0.01, 0.05, \text{ or } 0.001$ . We have not included the effect of uncertainties in parameters other than  $\sin^2(2\theta_{13})$  and  $\delta$ .

We have assumed that the JHF beam measures oscillation probabilities at 0.8 GeV, and the Fermilab beam at 9.0 GeV, although in reality a more sophisticated energy-dependent analysis will be performed. The expected oscillation probability measurements are shown in Table 2.

Constraints in the  $\sin^2(2\theta_{13})$ - $\delta$  plane from various combinations of these measurements are shown in Figs. 12 through 35. For each input value of  $\sin^2(2\theta_{13})$ , maximal CP violation can be detected at  $3\sigma$  or better, demonstrating a sensitivity over an impressive range of parameter space. This is possible since, as illustrated in Fig. 1, the maximum CP asymmetry is larger if  $\sin^2(2\theta_{13})$  is smaller, so the larger asymmetry provides statistical compensation for the smaller signal. Over most of this range, 2 years with the

Fermilab and JHF beams combined is enough to reach the  $3\sigma$  criterion. The constraints are improved with an 8 year run during which the JHF beam runs in antineutrino mode for 6 years. If the JHF antineutrino beam does not provide adequate performance, an 8 year run with Fermilab and JHF neutrino beams provides constraints almost as effective.

## 8 Summary and conclusions

We have investigated the physics potential of very long baseline experiments designed to measure  $\nu_\mu \rightarrow \nu_e$  oscillation probabilities. The principles of our design are to tune the beam spectrum to the resonance energy for the matter effect, and to have the spectrum cut off rapidly above this energy. The matter effect amplifies the signal, and the cut-off suppresses backgrounds which feed-down from higher energy. The signal-to-noise ratio is potentially better than for any other conventional  $\nu_\mu$  beam experiment.

The measurements from long- and short-baseline experiments are very complementary. The short-baseline experiment measures a CP-violating combination of atmospheric and solar oscillations. The relatively small matter effects can still confuse the interpretation of the measurements. At long baselines, solar oscillations play a relatively much smaller role. The long-baseline experiment determines the sign of  $\Delta M^2$ , constrains the matter effects, and constrains the size of the atmospheric  $\nu_\mu \rightarrow \nu_e$  oscillation alone.

In particular, we have investigated the capabilities of a neutrino beam from Fermilab aimed at the Super-K detector in Japan, 9300 km distant. At this baseline, neutrinos at the resonance energy have an oscillation probability 20 times the maximum in vacuum. We have used a simple model to estimate the signal efficiency and background, and it will be important to check this with a full simulation. For a normal mass hierarchy, a five year run can detect  $\sin^2(2\theta_{13})$  at  $3\sigma$  for values as low as 0.003. If the mass hierarchy is inverted, the beam can be run in antineutrino mode, with a similar signal-to-noise ratio, and event rate 55% as high as for the neutrino mode.

In an interesting coincidence for the 9300 km baseline, the second peak of maximum  $\nu_\mu$  disappearance occurs at the same energy as the peak for  $\nu_e$  appearance. Thus, interesting measurements of the parameters of  $\nu_\mu$  disappearance may also be possible.

Phase 2 of the JHF-Kamioka proposal assumes the construction of the Hyper-K detector with 40 times the fiducial mass of the Super-K detector.

Having this detector serve as the target for beams from both JHF and Fermilab is a powerful way of placing constraints in the  $\sin^2(2\theta_{13})$ - $\delta$  plane. We have investigated values of  $\sin^2(2\theta_{13})$  ranging from 0.001 to 0.05, and find that an 8 year run can establish maximal CP violation at  $3\sigma$  or better throughout this range. If the JHF antineutrino beam has poor performance, using Fermilab and JHF neutrino beams alone is almost as effective in constraining  $\delta$ .

## 9 Acknowledgments

We thank the NuMI collaboration for the use of their fast beamline simulation. In particular, we thank Debbie Harris for help with the use of this software.

## References

- [1] Y. Fukuda *et al.* [Super-Kamiokande Collaboration], Phys. Rev. Lett. **81**, 1562 (1998) [arXiv:hep-ex/9807003].
- [2] T. Kajita [Super-Kamiokande Collaboration], Nucl. Phys. Proc. Suppl. **100**, 107 (2001).
- [3] S. H. Ahn *et al.* [K2K Collaboration], Phys. Lett. B **511**, 178 (2001) [arXiv:hep-ex/0103001].
- [4] The MINOS collaboration, <http://www-numi.fnal.gov/>
- [5] M. B. Smy, arXiv:hep-ex/0202020.
- [6] A. Piepke [KamLAND Collaboration], Nucl. Phys. Proc. Suppl. **91**, 99 (2001).
- [7] G. Ranucci *et al.* [BOREXINO Collaboration], Nucl. Phys. Proc. Suppl. **91**, 58 (2001).
- [8] M. Apollonio *et al.* [CHOOZ Collaboration], Phys. Lett. B **466**, 415 (1999) [arXiv:hep-ex/9907037].
- [9] F. Boehm *et al.*, Phys. Rev. D **64**, 112001 (2001) [arXiv:hep-ex/0107009].

- [10] I. Mocioiu and R. Shrock, JHEP **0111**, 050 (2001) [arXiv:hep-ph/0106139].
- [11] I. Mocioiu and R. Shrock, AIP Conf. Proc. **533**, 74 (2000) [arXiv:hep-ph/9910554].
- [12] I. Mocioiu and R. Shrock, Phys. Rev. D **62**, 053017 (2000) [arXiv:hep-ph/0002149].
- [13] M. Freund, M. Lindner, S. T. Petcov and A. Romanino, Nucl. Phys. B **578**, 27 (2000) [arXiv:hep-ph/9912457].
- [14] A. Cervera, A. Donini, M. B. Gavela, J. J. Gomez Cadenas, P. Hernandez, O. Mena and S. Rigolin, Nucl. Phys. B **579**, 17 (2000) [Erratum-ibid. B **593**, 731 (2000)] [arXiv:hep-ph/0002108].
- [15] V. D. Barger *et al.*, arXiv:hep-ph/0103052.
- [16] V. D. Barger, S. Geer, R. Raja and K. Whisnant, Phys. Rev. D **63**, 113011 (2001) [arXiv:hep-ph/0012017].
- [17] V. D. Barger, D. Marfatia and K. Whisnant, in *Proc. of the APS/DPF/DPB Summer Study on the Future of Particle Physics (Snowmass 2001)* ed. R. Davidson and C. Quigg, arXiv:hep-ph/0108090.
- [18] C. Ankenbrandt *et al.*, Proton Driver Physics Study (Fermilab). <http://projects.fnal.gov/protondriver/>
- [19] Y. Itow *et al.*, arXiv:hep-ex/0106019.
- [20] J. J. Gomez-Cadenas *et al.* [CERN working group on Super Beams Collaboration], arXiv:hep-ph/0105297.
- [21] V. Barger, D. Marfatia and K. Whisnant, arXiv:hep-ph/0112119.
- [22] We thank Steve Geer for providing this calculation.
- [23] R. Alber *et al.*, <http://www-bd.fnal.gov/pdriver/reports.html>
- [24] Bill Foster, “8 GeV Injector Linac Study”, <http://tdserver1.fnal.gov/foster/>

- [25] We thank Jim Hylen for providing the fluxes from the full Geant simulations.
- [26] M. Aoki, K. Hagiwara, Y. Hayato, T. Kobayashi, T. Nakaya, K. Nishikawa and N. Okamura, arXiv:hep-ph/0112338.
- [27] G. Ingelman, A. Edin and J. Rathsman, Comput. Phys. Commun. **101**, 108 (1997) [arXiv:hep-ph/9605286].
- [28] H. Gallagher, presented at *NuInt01: The First International Workshop on Neutrino-Nucleus Interactions in the Few GeV Region*, December 13-16, 2001, KEK, Tsukuba, Japan.  
<http://neutrino.kek.jp/nuint01/>
- [29] V. D. Barger, S. Geer and K. Whisnant, Phys. Rev. D **61**, 053004 (2000) [arXiv:hep-ph/9906487].

Input values:  $\sin^2(2\theta_{13})=0.01$ ,  $\delta = \pi/2$ . Contours are 1, 2, 3 $\sigma$

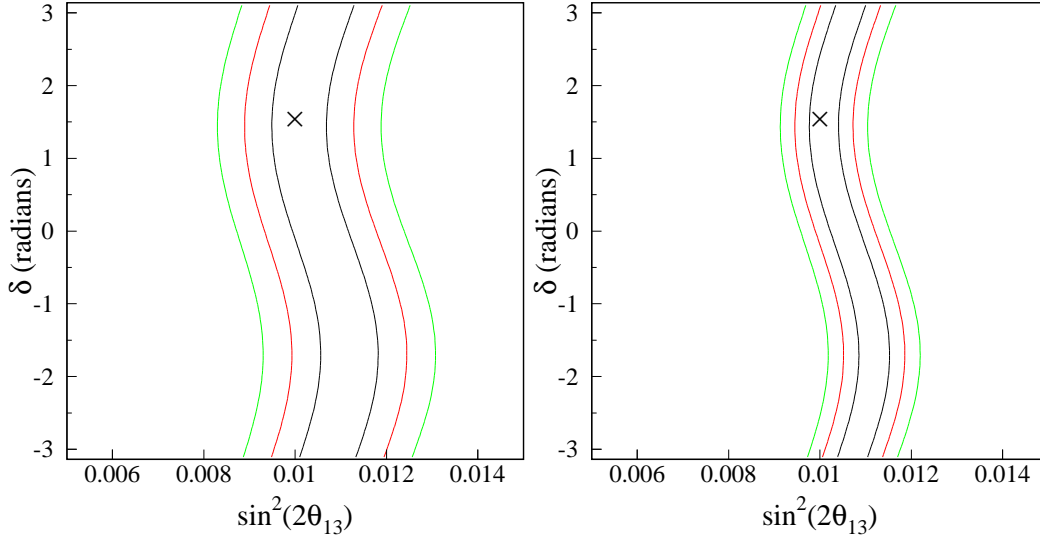


Figure 12: After 2 years with Fermilab beam.

Figure 13: After 8 years with Fermilab beam.

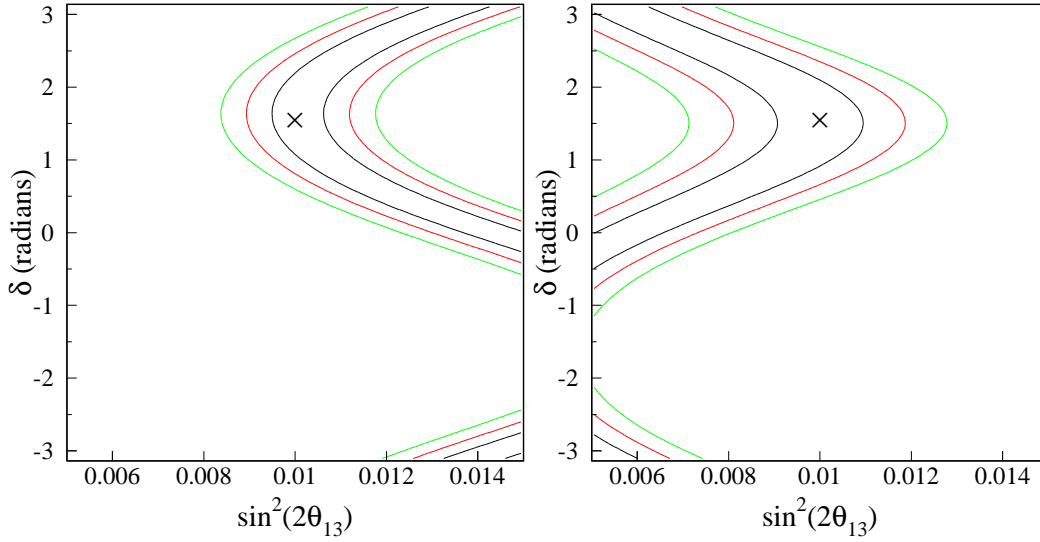


Figure 14: After 2 years with JHF beam.

Figure 15: After 6 years with JHF antineutrino beam.

Input values:  $\sin^2(2\theta_{13})=0.01$ ,  $\delta = \pi/2$ . Contours are 1, 2, 3 $\sigma$

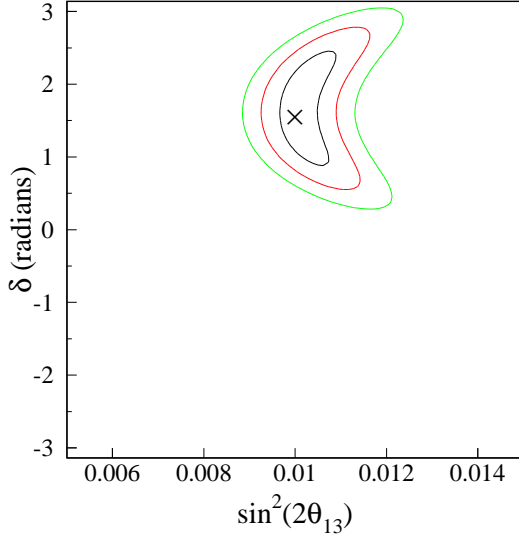


Figure 16: After 2 years with Fermilab and JHF beams.

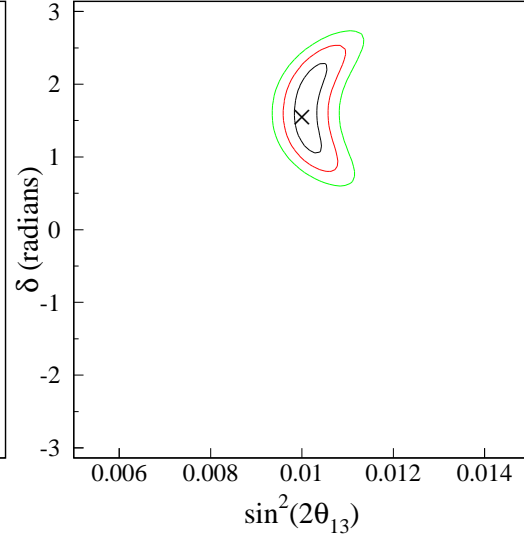


Figure 17: After 8 years with Fermilab and JHF beams.

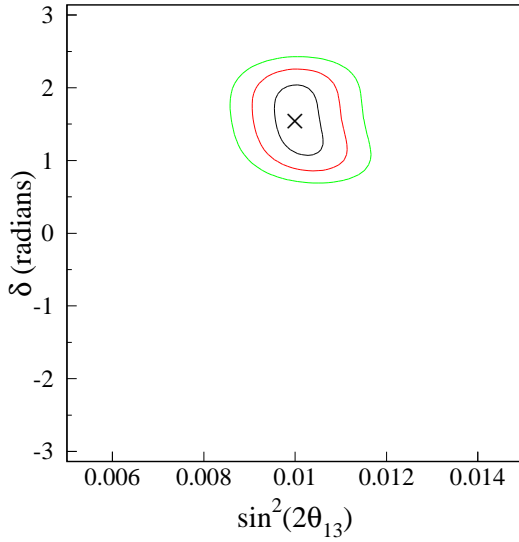


Figure 18: After 2 years with JHF beam and 6 years with JHF antineutrino beam.

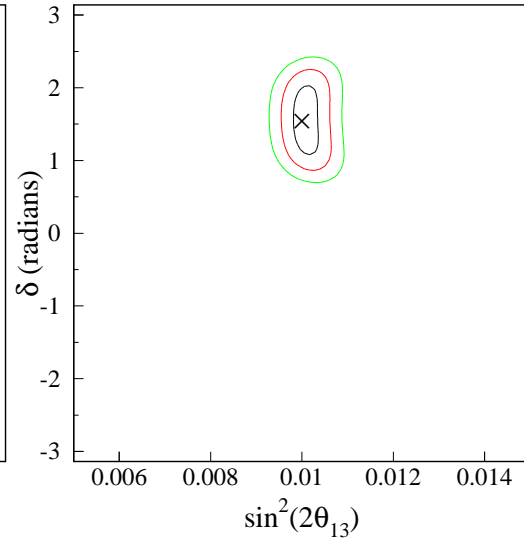


Figure 19: After 8 years with Fermilab, 2 years with JHF, and 6 years with antineutrino beams.



Input values:  $\sin^2(2\theta_{13})=0.05$ ,  $\delta = \pi/2$ . Contours are 1, 2, 3 $\sigma$

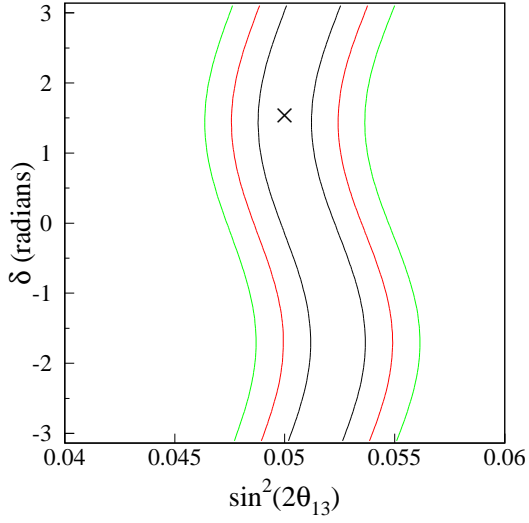


Figure 20: After 2 years with Fermilab beam.

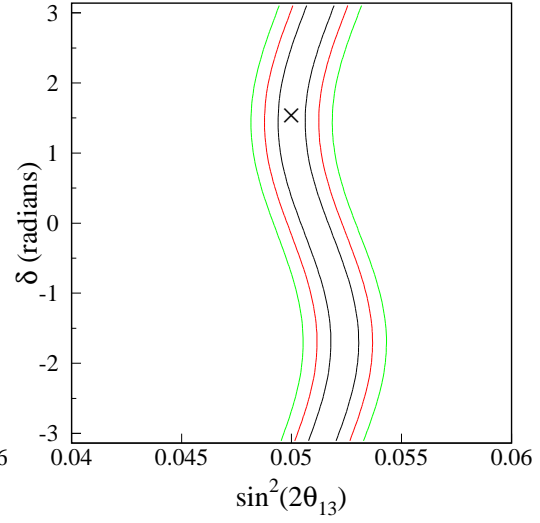


Figure 21: After 8 years with Fermilab beam.

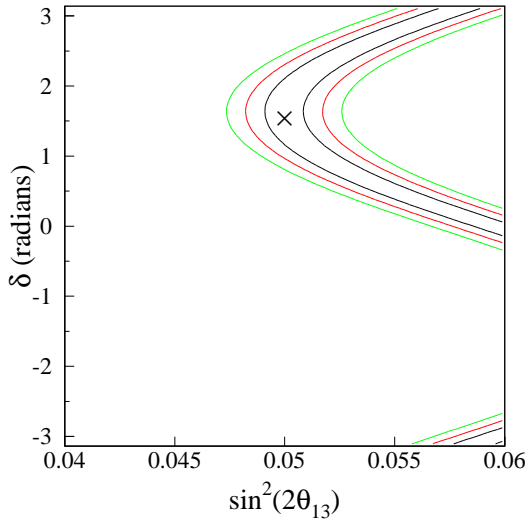


Figure 22: After 2 years with JHF beam.

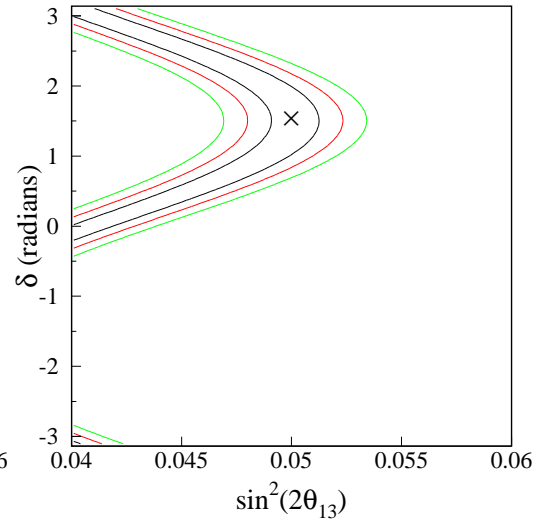


Figure 23: After 6 years with JHF antineutrino beam.

Input values:  $\sin^2(2\theta_{13})=0.05$ ,  $\delta = \pi/2$ . Contours are 1, 2, 3 $\sigma$

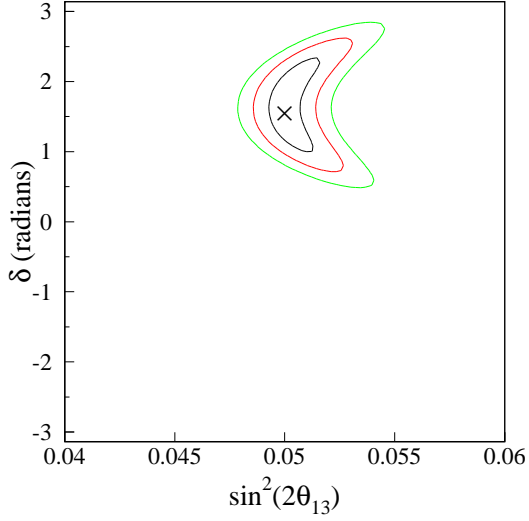


Figure 24: After 2 years with Fermilab and JHF beams.

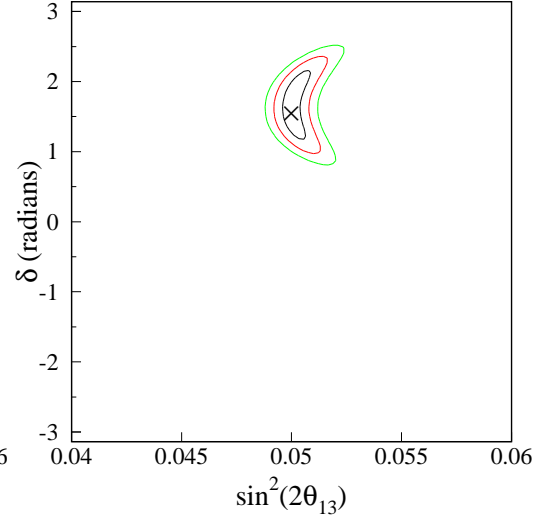


Figure 25: After 8 years with Fermilab and JHF beams.

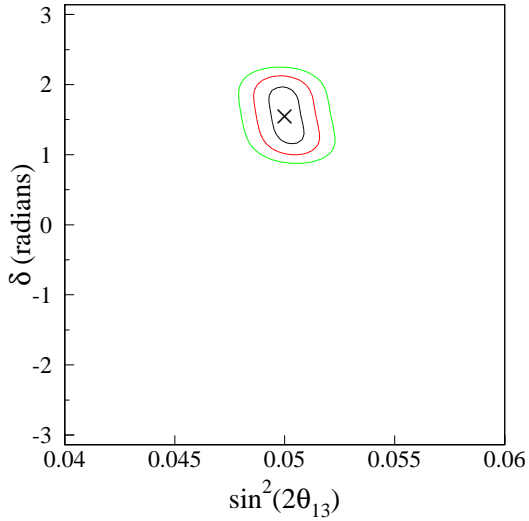


Figure 26: After 2 years with JHF beam and 6 years with JHF antineutrino beam.

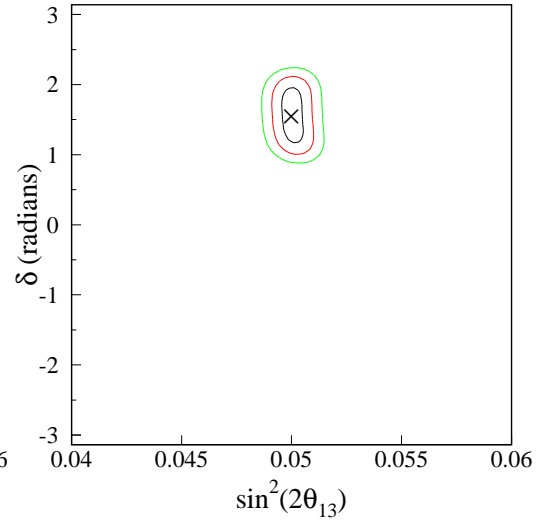


Figure 27: After 8 years with Fermilab, 2 years with JHF, and 6 years with antineutrino beams.

Input values:  $\sin^2(2\theta_{13})=0.001$ ,  $\delta = \pi/2$ . Contours are 1, 2, 3 $\sigma$

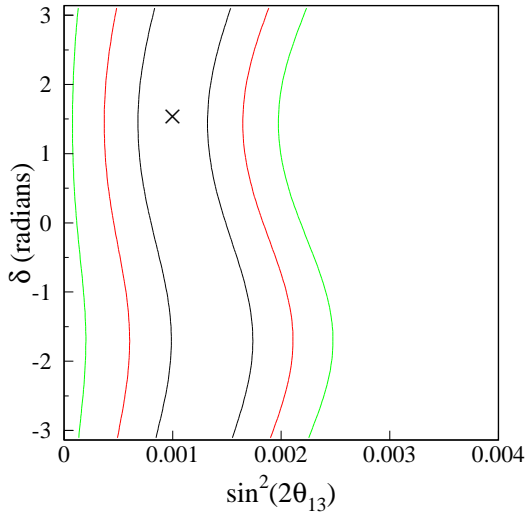


Figure 28: After 2 years with Fermilab beam.

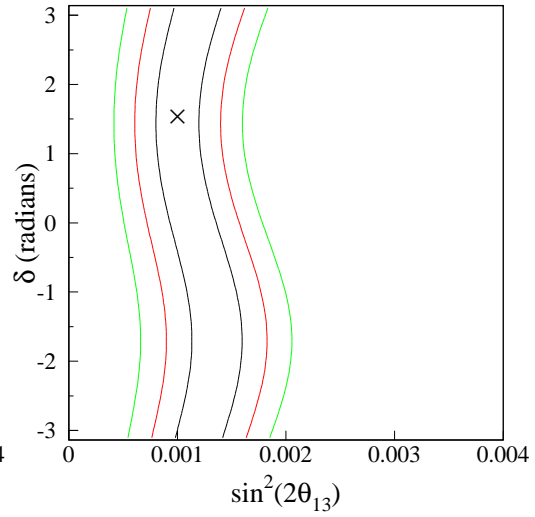


Figure 29: After 8 years with Fermilab beam.

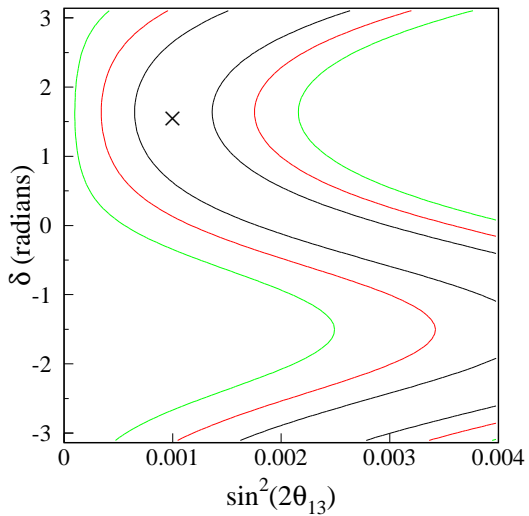


Figure 30: After 2 years with JHF beam.

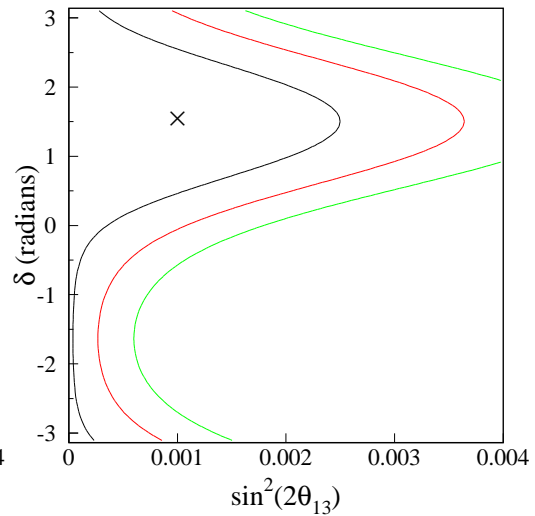


Figure 31: After 6 years with JHF antineutrino beam.

Input values:  $\sin^2(2\theta_{13})=0.001$ ,  $\delta = \pi/2$ . Contours are 1, 2, 3 $\sigma$

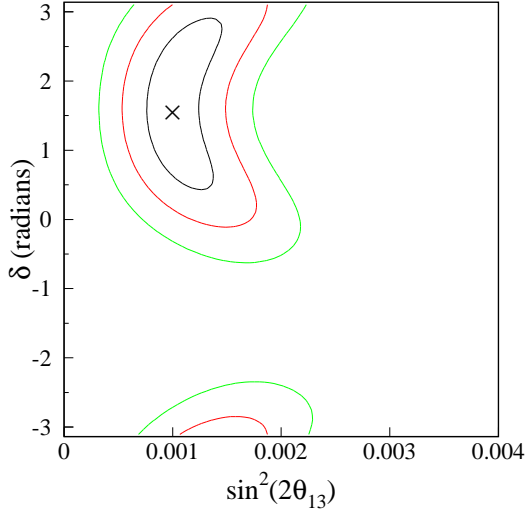


Figure 32: After 2 years with Fermilab and JHF beams.

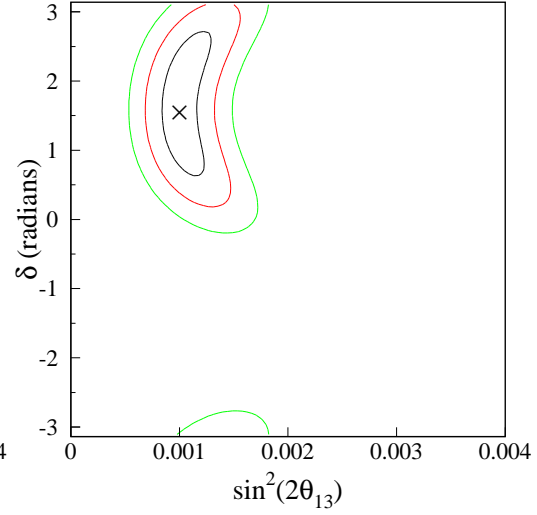


Figure 33: After 8 years with Fermilab and JHF beams.

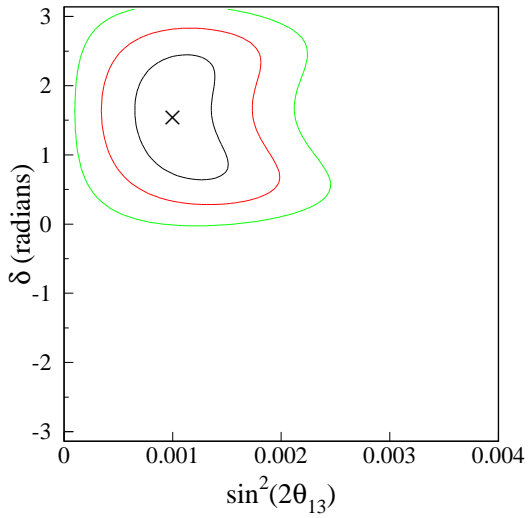


Figure 34: After 2 years with JHF beam and 6 years with JHF antineutrino beam.

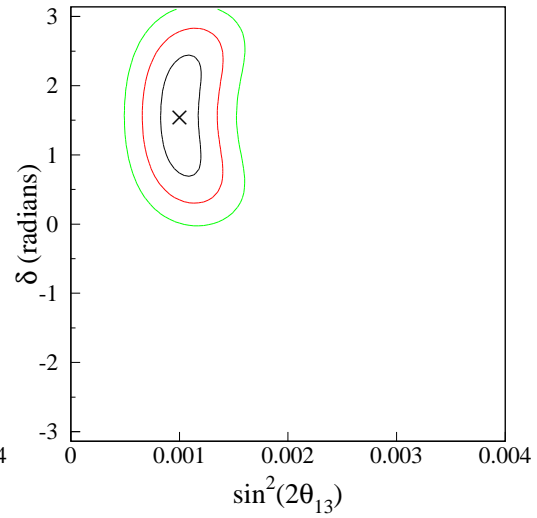


Figure 35: After 8 years with Fermilab, 2 years with JHF, and 6 years with antineutrino beams.